NeuroImage: Clinical 31 (2021) 102701

Contents lists available at ScienceDirect

NeuroImage: Clinical

journal homepage: www.elsevier.com/locate/ynicl

TSPO PET upregulation predicts epileptic phenotype at disease onset independently from chronic TSPO expression in a rat model of temporal lobe epilepsy

Daniele Bertoglio [a,b,*], Halima Amhaoul [b], Joery Goossens [b], Idrish Ali [b], Elisabeth Jonckers [c], Tom Bijnens [b], Matteo Siano [b], Leonie wyffels [a,d], Jeroen Verhaeghe [a], Annemie Van der Linden [c], Steven Staelens [b], Stefanie Dedeurwaerdere [e]

[a] Molecular Imaging Center Antwerp, University of Antwerp, Belgium
[b] Department of Translational Neurosciences, University of Antwerp, Belgium
[c] Bio-Imaging Lab, University of Antwerp, Belgium
[d] Department of Nuclear Medicine, Antwerp University Hospital, Edegem, Belgium
[e] Laboratory of Experimental Hematology, University of Antwerp, Belgium

ARTICLE INFO

Keywords:
Translocator protein
Inflammation
PET imaging
Neuroimaging
Kainic acid
KASE

ABSTRACT

Neuroinflammation is a key component of epileptogenesis, the process leading to acquired epilepsy. In recent years, with the development of non-invasive *in vivo* positron emission tomography (PET) imaging of translocator protein 18 kDa (TSPO), a marker of neuroinflammation, it has become possible to perform longitudinal studies to characterize neuroinflammation at different disease stages in animal models of epileptogenesis. This study aimed to utilize the prognostic capability of TSPO PET imaging at disease onset (2 weeks post-*SE*) to categorize epileptic rats with distinct seizure burden based on TSPO levels at disease onset and investigate their association to TSPO expression at the chronic epilepsy stage. Controls ($n = 14$) and kainic acid-induced *status epilepticus* (KASE) rats ($n = 41$) were scanned non-invasively with [^{18}F]PBR111 PET imaging measuring TSPO expression. Animals were monitored using video-electroencephalography (vEEG) up to chronic disease (12 weeks post-*SE*), at which TSPO levels ([^{3}H]PK11195) as well as other *post-mortem* abnormalities (namely synaptic density ([^{3}H]UCB-J), neuronal loss (NeuN), and neurodegeneration (FjC)) were investigated. By applying multivariate analysis, TSPO PET imaging at disease onset identified three KASE groups with significantly different spontaneous recurrent seizures (SRS) burden (defined as rare SRS, sporadic SRS, and frequent SRS) ($p = 0.003$). Interestingly, TSPO levels were significantly different when comparing the three KASE groups ($p < 0.0001$), with the frequent SRS group characterized only by a limited focal TSPO increase at disease onset. On the contrary, TSPO measured during chronic epilepsy was found to be the highest in the frequent SRS group and correlated with seizure burden ($r = 0.826$, $p < 0.0001$). Importantly, early and chronic TSPO levels did not correlate ($r = -0.05$). Finally, significant pathological changes in neuronal loss, synaptic density, and neurodegeneration were found not only when compared to control animals ($p < 0.01$), but also between the three KASE rat categories in the hippocampus ($p < 0.05$). Early and chronic TSPO upregulation following epileptogenic insult appear to be driven by two superimposed dynamic processes. The former is associated with epileptogenesis as measured at disease onset, while the latter is related to seizure frequency as quantified during chronic epilepsy.

1. Introduction

Temporal lobe epilepsy (TLE) is the most common focal and pharmacoresistant form of epilepsy in adults, accounting for approximately 60% of all partial epilepsies (Engel, 1996; Tellez-Zenteno and Hernandez-Ronquillo, 2012). The clinical hallmark of TLE is the occurrence of spontaneous recurrent seizures (SRS) in parallel to a high prevalence of neuropsychiatric comorbid disorders, such as depression and anxiety (Keezer et al., 2016), severely affecting the patient's quality of life.

* Corresponding author at: Molecular Imaging Center Antwerp, University of Antwerp, Belgium.
E-mail address: daniele.bertoglio@uantwerpen.be (D. Bertoglio).

https://doi.org/10.1016/j.nicl.2021.102701
Received 3 March 2021; Received in revised form 10 May 2021; Accepted 14 May 2021
Available online 28 May 2021

TLE can be acquired following epileptogenesis, a process during which an initial brain insult (such as *status epilepticus* (*SE*), brain trauma, or stroke) triggers a series of pathophysiological changes, including brain inflammation, abnormal neuronal network reorganization, and synaptic circuit alterations (Ben-Ari, 2001; Goffin et al., 2008; Lillis et al., 2015), ultimately leading to the development of SRS and neuropsychiatric comorbidities (Pitkanen and Engel, 2014). The latent period between the initial epileptogenic insult and the appearance of clinically relevant symptoms can last from a few months to several years (Pitkanen et al., 2015).

In recent years, the relevance of neuroinflammation during epileptogenesis (Koepp et al., 2017; Ravizza et al., 2011; Vezzani et al., 2011, 2013b; Vezzani and Friedman, 2011) as well as during chronic epilepsy (Vezzani et al., 2011) has been postulated and reported in animal models of TLE (Amhaoul et al., 2015; Auvin et al., 2010; Brackhan et al., 2016; Pernot et al., 2011). In particular, translocator protein 18 kDa (TSPO) (Rupprecht et al., 2010) represents a candidate *in vivo* biomarker to study neuroinflammation as it can be imaged non-invasively utilizing positron emission tomography (PET) with several radioligands, including [^{18}F]PBR111, [^{18}F]DPA714, and [^{18}F]GE180. Several preclinical studies focusing on TSPO PET imaging during epileptogenesis have demonstrated its potential as a possible non-invasive *in vivo* marker of epileptogenesis (Bertoglio et al., 2017b; Brackhan et al., 2016, 2018; Dedeurwaerdere et al., 2012; Nguyen et al., 2018; Russmann et al., 2017).

In the well-established kainic acid-induced *status epilepticus* (KASE) rat model of TLE (Levesque and Avoli, 2013), we have previously reported that TSPO expression during epileptogenesis peaks around 1 to 2 weeks post-*SE*, it is mainly associated with microglia activation (Amhaoul et al., 2015; Bertoglio et al., 2017a), and can be quantified using [^{18}F]PBR111 PET imaging (Amhaoul et al., 2015; Dedeurwaerdere et al., 2012). Additionally, we demonstrated that a single TSPO PET scan at disease onset (2 weeks post-*SE*) could accurately predict the SRS frequency KASE rats will develop during chronic epilepsy (Bertoglio et al., 2017b), indicating its potential prognostic value for the stratification of subjects at risk. Using this powerful paradigm, this study aims to investigate the association of TSPO expression at disease onset with TSPO levels during chronic epilepsy as well as seizure frequency by stratifying epileptic rats into three distinct seizure burden groups based on our previous work (Bertoglio et al., 2017b). Additionally, we assessed different neuropathology read-outs and their relationship with TSPO levels during chronic epilepsy.

2. Materials and methods

2.1. Animals

A total of 55 male Wistar Han rats (Charles River Laboratories, France) were purchased at 5 weeks of age. Animals were individually housed under a 12 h light/dark cycle in a temperature- (22 ± 2 °C) and humidity-controlled (55 ± 10%) environment with food and water available *ad libitum*. A minimum of five days was provided to the animals before the start of the procedures to acclimatize. All procedures were performed according to the European Committee (2010/63/EU) and the Animal Welfare Act (7 USC 2131). All of the animal experiments were approved by the ethical committee for animal testing (ECD 2014–39) at the University of Antwerp (Belgium).

2.2. Experimental design

An overview of the experimental workflow is reported in Fig. 1. Briefly, 14 days following induction of *SE* (controls, $n = 14$; KASE rats, $n = 41$), animals underwent a [^{18}F]PBR111 PET scan to measure TSPO levels at disease onset (occurrence of the first spontaneous seizure). Next, we applied principal component analysis on the TSPO PET dataset to identify clusters of KASE subgroups. Then, we predicted the SRS frequency of the animals using partial least square (PLS) regression and divided the KASE animals into three groups depending on the estimated SRS frequency (namely KASE – rare SRS, KASE – sporadic SRS, and KASE – frequent SRS). Finally, we investigated *in vivo* inter-regional TSPO patterns at disease onset as well as *post-mortem* histopathological changes 12 weeks post-*SE* (chronic disease) among the three KASE groups. Specifically, we assessed neuroinflammation and synaptic density using autoradiography ([^{3}H]PK11195 and [^{3}H]UCB-J, respectively) as well as neuronal loss and neurodegeneration with NeuN immunohistochemistry and Fluorojade C immunofluorescence respectively. Finally, associations between variables were investigated.

This study focused on stratification of KASE rats depending on their epileptic outcome, thus we allocated more animals to the KASE group ($n = 41$) than the control group ($n = 14$), still providing an appropriate sample size for statistical comparison. Additionally, animals were divided into two main groups. The first group of animals (controls, $n = 7$; KASE rats, $n = 15$) was used to describe the capability of [^{18}F]PBR111 PET scan 14 days post-*SE* in predicting SRS outcome. These animals were implanted with MRI-compatible epidural electrodes 2 weeks before induction of *SE* and were vEEG monitored continuously (24/7) during the entire study (12 weeks) to reliably predict the SRS frequency for each subject. The resulting *in vivo* data for those animals were

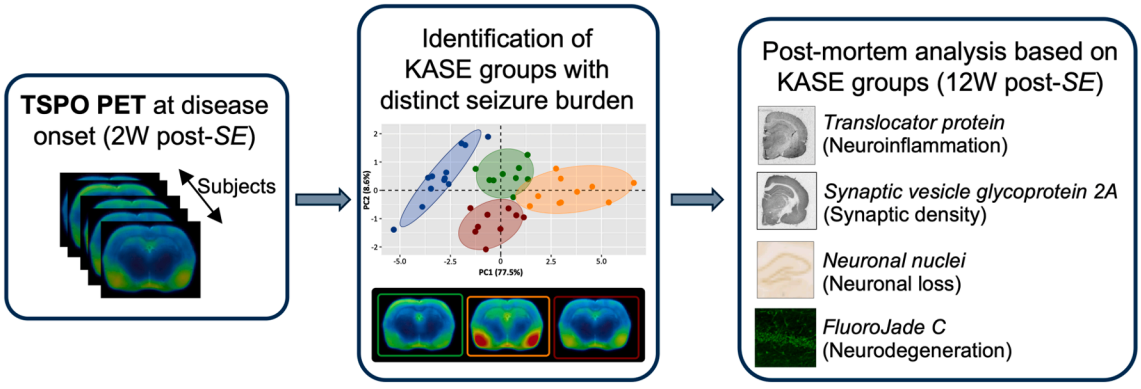

Fig. 1. Flowchart of the analysis. Following induction of *SE* (controls, $n = 14$; KASE rats, $n = 41$), animals underwent a TSPO PET scan at disease onset (14 days post-*SE*). Next, principal component analysis (PCA) was applied on the TSPO PET data to identify KASE subgroups representing different SRS outcome categories, and the spontaneous recurrent seizures (SRS) frequency for each individual was predicted by partial least square (PLS) regression. TSPO levels at disease onset as well as during chronic epilepsy (12 weeks post-*SE*) were explored in the KASE categories. Additionally, different *post-mortem* histopathological features at chronic disease were investigated and their association with TSPO levels was assessed.

previously published (Bertoglio et al., 2017b) and used in the current study to predict the SRS outcome of a second large cohort (controls, $n = 7$; KASE rats, $n = 15$). This second group of animals was implanted with epidural electrodes during the chronic phase of the disease (8 weeks post-*SE*) and were vEEG monitored continuously (24/7) for a total of 2 weeks during the chronic phase.

2.3. Induction of status epilepticus

A total of 14 animals were randomly assigned to the control group, while the remaining 41 were allocated to the KASE group. Induction of *SE* was performed using a low-dose kainic acid (KA, A.G. Scientific, USA) protocol with the procedure we previously reported (Bertoglio et al., 2017a, 2017b). On the date of the induction, control animals displayed a bodyweight of 220.5 ± 25 g, while KASE rats were 221.8 ± 28 g. The average administered KA dose was 18.4 ± 6.0 mg/kg. One animal did not reach *SE* (97.5% induction rate) and four animals did not survive the *SE* (10% mortality rate). Additionally, two KASE rats did not recover from *SE* and were euthanatized in the following days. These animals were excluded from all analyses.

2.4. Anatomical T_2 MRI

T_2 MRI scans were performed on a 9.4 T Biospec scanner (Bruker, Germany) in the same week of PET/CT scan with the same procedure previously described (Bertoglio et al., 2017b). Animals were anesthetized using isoflurane (Forene, Belgium) in a mixture of N_2/O_2 (induction 5%, maintenance 2.5%) and placed in a prone position into the scanner. Body temperature was maintained constant by using a rectal thermistor with feedback-controlled warm air circuitry (MR-compatible Small Animal Heating System, SA Instruments, Inc., USA). Respiration rate was also monitored throughout the experiment using a pressure-sensitive sensor under the rat (MR-compatible Small Animal Monitoring and Gating System, SA Instruments, Inc., USA). After a Tripilot scout image, a rapid acquisition with relaxation enhancement (RARE) sequence was used to obtain 70 coronal slices with a 0.4 mm thickness ($0.17 \times 0.114 \times 0.35$ mm^3 voxels), an acquisition matrix of 256×344, and a field of view (FOV) of $30 \times 40 \times 28$ mm^2. The MR image acquisition procedure lasted for about 10 min, after which the animals were placed in a recovery box while heated under an infrared lamp. All data were acquired using ParaVision 5.1 (Bruker, Germany). Volumes of interest (VOIs) were manually delineated for each animal in PMOD 3.6 software (Pmod Technologies, Zurich, Switzerland) to correct for possible hippocampal sclerosis when quantifying [^{18}F]PBR111 PET images. The following VOIs were considered: whole brain (WB), olfactory bulb (OLF), frontal cortex (FC), insular cortex (INS), hippocampus (HC), extrahippocampal temporal lobe (TEMP), ventricles (VENT), piriform cortex (PIR), thalamus (THAL), and cerebellum (CB).

2.5. TSPO PET imaging

TSPO was visualized using the radioligand [^{18}F]PBR111. Synthesis of [^{18}F]PBR111 was achieved using a Fluorsynton I automated synthesis module (Comecer Netherlands, The Netherlands) as previously described (Bourdier et al., 2012) with a molar activity of 206.4 ± 30.2 GBq/μmol. MicroPET/Computed tomography (CT) images were acquired using two virtually identical Siemens Inveon PET/CT scanners (Siemens Preclinical Solution, Knoxville, USA). Animal preparation was performed as previously described (Bertoglio et al., 2017b). Briefly, rats were anesthetized using isoflurane in medical oxygen (induction 5%, maintenance 2–2.5%). The respiration rate of the animal was monitored during the entire scan and body temperature was maintained constant using a feedback-controlled warm air circuitry (Minerve, France). The radioligand was injected into the tail vein of the animal using an automated pump (Pump 11 Elite, Harvard Apparatus, USA) over 1-min. Animals were injected 10.5 ± 2.0 MBq [^{18}F]PBR111 corresponding to a cold mass of 0.28 ± 0.02 nmol/kg. One control and two KASE rats were excluded from the analysis because of faulty tracer injection.

Immediately after the PET scan, a 10 min 80 kV/500 μA CT scan was performed for attenuation correction and co-registration purposes. Iterative PET image reconstruction was performed after Fourier rebinning (Defrise et al., 1997) using an ordered-subset expectation–maximization algorithm (OSEM-2D) (Hudson and Larkin, 1994) including corrections for normalization, dead-time, attenuation, and random coincidences provided by the manufacturer. PET image frames were reconstructed on a $128 \times 128 \times 159$ grid with $0.776 \times 0.776 \times 0.796$ mm^3 voxels.

Image analysis and processing of the data was performed in PMOD 3.6 software (Pmod Technologies, Zurich, Switzerland). Registration of the CT and PET images to the individual MRI was achieved by automated rigid matching of the individual CT images to the correspondent MRI. Since PET and CT images were acquired on the same gantry, the same automated rigid matching was applied to co-register PET and MR images. All images were visually checked for accuracy. The time window of 45 to 60 min post-injection of the radiotracer was used for measurement of the TSPO levels as standardized uptake value (SUV), calculated as the concentration of radioactivity in the tissue divided by the injected radioactivity over the body weight of the animal. The tissue radioactivity was extracted using the VOIs manually delineated on the individual MR images. Finally, average SUV images for each investigated group were obtained by averaging the SUV images of animals assigned to the category (i.e. controls, KASE – rare SRS, KASE – sporadic SRS, and KASE – frequent SRS).

2.6. Principal component analysis

Principal Component Analysis (PCA) is a data reduction method that determines a set of linearly uncorrelated components that account for multi-dimensional variability in a dataset. The following brain regions were included in the analysis: FC, INS, THAL, HC, PC, TEMP, OB, CB, and VENT. The two-dimensional PCA accounted for a total of 86.1% of the total variance of the data (PC1 = 77.5% and PC2 = 8.6%). INS, TEMP, and VENT contributed to dimension 1 (PC1), while FC was the main contributor to dimension 2 (PC2). Given the large dataset ($n = 40$), the resulting subject-to-variable ratio was 4.4, well above the recommended ratio of 1.2 to obtain satisfactory results (Barrett and Kline, 1981), indicating an adequate sample size for PCA.

2.7. Partial least squares regression

PLS regression, a method for constructing predictive models based on highly collinear factors, was applied to predict the SRS frequency of KASE animals scanned at disease onset by regressing the independent variables (factors, i.e. regional [^{18}F]PBR111 uptake) on the dependent variable (response, i.e. SRS/day) and vice versa (Naes and Martens, 1985). As we previously demonstrated that PLS regression can be applied to [^{18}F]PBR111 PET imaging at disease onset to identify SRS frequency in KASE rats (Bertoglio et al., 2017b), we extended the approach to a larger dataset and to determine three SRS categories (KASE – Rare SRS = 0.08 [0.028, 0.15] SRS/day, KASE – Sporadic SRS = 0.17 [0.11, 0.22] SRS/day, and KASE – Frequent SRS = 0.62 [0.27, 0.87] SRS/day). A quasi-Poisson distribution was used to account for count data and overdispersion. The optimal number of components was obtained by cross-validation (Gomez-Carracedo et al., 2007).

2.8. Electrode implantation

Electrodes were implanted on all animals two weeks before the start of the vEEG recordings to guarantee an adequate recovery time. Rats that underwent 12 weeks vEEG recording (controls, $n = 6$; KASE rats, $n = 15$) were implanted with an MRI-compatible epidural tripolar electrode (Bilaney Consultants, Plastics One Inc., Germany) as already

described (Bertoglio et al., 2017b). Animals monitored only during chronic epilepsy (10 weeks post-*SE*) (controls, $n = 7$; KASE rats, $n = 15$) were implanted with four surface Teflon-coated stainless steel wires electrodes (330 μm; Science Products, Germany), soldered to a gold-plated connector pin at one end, and a stainless-steel screw on the other end (PlasticsOne, Bilaney Consultants, Germany). Connector pins from all electrodes were mounted into a protective plastic pedestal (PlasticsOne, Bilaney Consultants, Germany), and the entire assembly was insulated and fixed to the cranium with dental cement (Simplex Rapid, Kemdent, UK & Durelon, 3 M ESPE, USA) as previously described (Amhaoul et al., 2015). Following the surgery, xylocaine (2%; AstraZeneca, Belgium) was locally applied to the wound, buprenorphine (0.01 mg/kg, subcutaneously (s.c.); Ecuphar, the Netherlands) injected for pain relief, and Hartmann's solution (10 ml/kg, s.c.; Viaflo Baxter Healthcare, Belgium) administered to prevent dehydration. Animals were returned to their home cages for recovery and placed under an infrared lamp. Additional care was taken over the days following surgery, with the animals receiving enriched soft food pellets and Hartmann's solution (10 ml/kg, s.c.) if needed.

2.9. vEEG recording

Freely moving control and KASE rats were subjected to continuous vEEG for the recording period as previously described (Amhaoul et al., 2015; Bertoglio et al., 2017b). Animals were connected to the digital EEG acquisition system (Ponemah P3 Plus; Data Sciences International, USA) using a three-channel connector cable with a spring and a rotor-containing commutator (Bilaney Consultants, Plastic One Inc., Germany). Besides, a network video camera (Axis P1343, Axis Communications, Sweden), coupled with a night-vision infrared lamp (Raymax 25 IP, Raytec, UK) used to improve video quality during the lights-off period, was synchronized to the EEG acquisition system.

vEEG recordings were manually analysed for SRS identification by an experienced investigator using Neuroscore 3.0 (Data Sciences International, USA) as previously reported (Williams et al., 2009). Besides, synchronized video-recordings were used to visually classify SRS severity using the behavioural scale of Racine (Racine, 1972) as previously described (Bertoglio et al., 2017a). The number of SRS per day was determined for statistical analysis. Three rats lost their electrode assembly before the conclusion of the vEEG period and they were euthanized before the study endpoint to avoid discomfort.

2.10. Tissue collection

At 12 weeks post-*SE*, controls ($n = 13$) and KASE rats ($n = 30$) were rapidly decapitated. Brains were immediately dissected, snap-frozen in 2-methylbutane at −35 °C for 3 min, and further preserved at −80 °C. Serial coronal sections of 20 μm thickness of the dorsal hippocampus were collected in triplicate starting at bregma −2.40 mm (Paxinos and Watson, 2007), on positively charged glass slides (Menzel-Gläser, Thermo Fischer Scientific, USA) using a cryostat (Leica, Germany). All *post-mortem* analyses were performed on consecutive slides at bregma −3.00 mm to visualize the dorsal hippocampus and piriform cortex because of their high interconnectivity with other limbic nuclei, playing a key role in seizure generation and propagation in TLE.

2.11. Autoradiography

In vitro autoradiography was performed to quantify neuroinflammation and synaptic density using the TSPO ligand [^{3}H]PK11195 (PerkinElmer, USA) as previously described (Bertoglio et al., 2017a) and synaptic vesicle glycoprotein 2A (SV2A) ligand [^{3}H]UCB-J (Novandi Chemistry AB, Sweden), respectively. First, sections were air-dried at room temperature, re-incubated for 20 min with binding buffer (50 mM Tris-HCl buffer, pH 7.4), and dried using a warm airflow. Next, consecutive slides were incubated with either total binding solution (TB, 1 nM of [^{3}H]PK11195 or [^{3}H]UCB-J in binding buffer) or non-specific binding solution (NB, 1 nM of [^{3}H]PK11195 + 40 μM of cold PK11195 or [^{3}H]UCB-J + 10 μM of cold UCB-J in binding buffer) for 1 h at room temperature. Subsequently, sectioned were washed in the binding buffer on ice, dipped into distilled water, and dried for 2 h at room temperature. Sections and tritium standards (American Radiolabelled Chemicals Inc., USA) were exposed for 6 weeks to Amersham Hyperfilm MP (GE Life Sciences, Belgium). Autoradiographic films were developed manually and digitalized using an Epson V700 photo scanner (Seiko Epson Corporation, Japan).

Regions-of-interest (ROIs) were manually delineated in triplicate for CA1, HC, PIR, and TEMP by an experienced investigator blind to condition using Fiji - ImageJ software (National Institute of Health, USA). Regional specific binding was quantified by subtracting the non-specific binding from the total binding (in Bq/mg tissue) divided by the decay-corrected molar activity of the radioligand (in Gb/μmol) on an experimental day to obtain the final value (number of mol/mg) for statistical analysis.

2.12. Histology

Histological assessment was performed to evaluate the neuronal loss and ongoing neurodegeneration by visualizing neuronal nuclei (NeuN) and fluorojade C (FjC), respectively. NeuN immunostaining was executed as previously described (Bertoglio et al., 2017a). Briefly, following an initial fixation step (4% paraformaldehyde, PFA, for 10 min) and blocking (0.5% Triton-X and 5% normal donkey serum, NDS, for 20 min) sections were incubated overnight with the mouse anti-rat NeuN primary antibody (1:2000, Merck Millipore, Germany) in blocking solution. The next day, sections were incubated with peroxidase-conjugated donkey anti-mouse antibody (IgG-HRP, 1:500, Jackson Immunoresearch, UK) in antibody diluent for 1 h, after which they were exposed for 10 min to the colorimetric diaminobenzidine marker. Finally, sections were dehydrated and coverslipped. Images were acquired with a NanoZoomer-ZR slide scanner (Hamamatsu, Japan) equipped with a 20X objective and processed with the Pannoramic Viewer (3DHISTECH Ltd, Hungary). Neuronal density was measured using Fiji - ImageJ software (National Institute of Health, USA) in CA1 and PC by converting them into grayscale (8-bit) and applying an intensity threshold to all images to remove the background signal. The intensity threshold, and the minimum and maximum cell size parameter values were initially determined empirically. The outcome of the analysis was the total number of positive cells in the field of view, performed blinded to condition on triplicate sections of which the mean score was considered for statistical analysis.

FjC staining was executed to determine ongoing neurodegeneration as previously reported (Bertoglio et al., 2017a; Schmued et al., 2005). Briefly, after an initial fixation step (4% PFA for 10 min), sections were dipped into a 1% sodium hydroxide in 80% ethanol solution for 5 min, rinsed in 70% ethanol for 2 min, and immersed into 0.06% potassium permanganate solution for 10 min. Next, sections were transferred into a solution of 0.0005% FjC (Merck Millipore, Germany) dissolved in 0.1% acetic acid. Finally, sections were dehydrated and coverslipped. Images of CA1 and PC were acquired in triplicate at 20X with a fluorescent microscope (Olympus, Japan) using Olympus CellSens software. The total number of FjC positive cells was visually counted by two independent investigators blind to the condition. The mean value of each region was considered for statistical analysis.

2.13. Statistical analysis

All data were assessed for normal distribution using the D'Agostino-Pearson omnibus normality test. [^{18}F]PBR111 data were normally distributed, therefore an unpaired *T*-test was applied to compare controls and KASE rats. Besides, one-way ANOVA with Holm-Sidak *post-hoc* correction for multiple comparisons was used to analyse [^{18}F]PBR111

data when KASE rats were divided into KASE categories. For all the other variables, the Mann-Whitney *U* test was applied for comparison between controls and all KASE rats. To investigate differences among controls and KASE categories, we used the Kruskal-Wallis test with *post-hoc* Dunn's multiple comparison test. Spearman rank correlation tests were applied to examine the relationship between measurements, exemplified by piriform cortex. All the above analyses were performed using GraphPad Prism (v8.4) statistical software. PCA and PLS regression were performed in RStudio (version 1.2 build 1351), using the *factoextra* and *pls* packages, respectively. For consistency, all data are represented as median ± 95% confidence intervals (CI). All tests were two-tailed, and significance was set at $p < 0.05$.

3. Results

3.1. TSPO levels at disease onset identify categories of KASE rats with different seizure burden

TSPO levels were measured non-invasively using [^{18}F]PBR111 PET imaging 2 weeks post-*SE*. [^{18}F]PBR111 uptake was significantly higher in KASE rats compared to control animals in all investigated brain regions with the largest difference observed in the extra-hippocampal temporal lobe (controls = 0.51 [0.47, 0.54], KASE rats = 1.48 [1.23, 1.73], $p < 0.0001$) (Fig. S1a). Given the variability among KASE rats, we applied PCA, which distinguished 3 independent clusters of KASE rats (Fig. 2a). Based on our *a posteriori* knowledge of the SRS outcome for half of the animals ($n = 15$), we could categorize the 3 clusters of KASE animals according to the future SRS burden they will experience with the progression of the disease (i.e. 'Rare SRS', 'Sporadic SRS', and 'Frequent SRS') and estimate the different SRS frequency among the KASE categories (KASE – Rare SRS = 0.08 [0.028, 0.15] SRS/day, KASE – Sporadic SRS = 0.17 [0.11, 0.22] SRS/day, and KASE – Frequent SRS = 0.62 [0.27, 0.87] SRS/day; $p = 0.003$) with a significant *post-hoc* difference between KASE – Frequent SRS versus KASE – Rare SRS ($p = 0.0002$) as well as KASE – Sporadic SRS ($p = 0.0449$) (Fig. 2b). Average [^{18}F]PBR111 SUV PET images for the four experimental groups (Fig. 2c) depicted the elevated yet different [^{18}F]PBR111 binding in the temporal lobe and hippocampus of KASE rats categories. Accordingly, TSPO levels were significantly different among groups (e.g. in temporal lobe, $F_{3,36} = 92.73$, $p < 0.0001$). Interestingly, [^{18}F]PBR111 uptake in KASE – Sporadic SRS was significantly higher than the other KASE categories ($p < 0.0001$) (Fig. 2d). The distinct TSPO cerebral distribution pattern across KASE categories was also visible in their correlation matrices (Fig. S2).

3.2. TSPO levels at disease onset and during chronic epilepsy are independent

TSPO levels 12 weeks post-*SE* were measured using *in vitro* [^{3}H] PK11195 autoradiography. Similar to the finding at 2 weeks post-*SE*, TSPO levels were significantly higher in KASE animals compared to control rats in all investigated regions (e.g. in PIR: controls = 82.5 [30.5, 106.8] fmol/mg; KASE rats = 194.1 [94.1, 254.3] fmol/mg, +135%, $p < 0.01$) (Fig. S1b). Nonetheless, when considering the different KASE categories, TSPO levels during the chronic period increased significantly with the SRS frequency of the KASE rats (Fig. 2e), unlike what was observed at disease onset (Fig. 2d). Accordingly, no association between TSPO measurements at disease onset and chronic epilepsy was observed, as exemplified by piriform cortex ($r = -0.05$, $p = 0.79$) (Fig. 2f). In addition, TSPO levels measured at 2 weeks post-*SE* in individual brain structures did not correlate with seizure frequency ($r = -0.12$, $p = 0.52$) (Fig. 2g), unlike TSPO measurement at 12 weeks post-*SE*, which was strongly associated ($r = 0.826$, $p < 0.0001$) (Fig. 2h).

3.3. Post-mortem assessment during chronic disease

In addition to TSPO levels, neuronal loss, neurodegeneration, and SV2A density were assessed 12 weeks post-*SE*. In terms of neuronal loss, KASE rats displayed a significantly reduced neuronal count compared to controls in both the CA1 and PIR (e.g. in PIR: controls = 524.3 [489, 585.4] counts; KASE rats = 303.0 [256.0, 336.3] counts, −42.2%, $p < 0.0001$) (Fig. S3a). Representative NeuN images of CA1 in control and KASE – Frequent SRS rats are depicted in Fig. 3a. KASE rats in the different categories did not differ from each other (Fig. 3b), nonetheless, a negative correlation with TSPO levels was observed ($r = -0.649$, $p = 0.0003$) (Fig. 3c).

KASE rats also displayed a significantly higher number of degenerating neurons compared to control animals in both the CA1 and PIR (e.g. in PIR: controls = 0.0 [0.0, 1.3] positive cells; KASE rats = 37.3 [4.0, 68.0] positive cells, $p < 0.0001$) (Fig. S3b). Representative FjC images of CA1 in control and KASE – Frequent SRS rats are shown in Fig. 3d. When considering the different KASE categories, FjC positive cell count was different among groups ($p < 0.0001$) with the KASE rats with Frequent SRS displaying significantly higher neurodegeneration compared to controls ($p = 0.0003$) and KASE rats – Rare SRS ($p = 0.039$) (Fig. 3e). Interestingly, neurodegeneration levels were also associated to TSPO expression (e.g. PIR: $r = 0.713$, $p < 0.0001$) (Fig. 3f).

Finally, SV2A density was significantly reduced in KASE rats compared to control animals in the hippocampus (e.g. in CA1: controls = 406.5 [392.7, 441.1] fmol/mg; KASE rats = 289.3 [241.4, 339.8] fmol/mg, −28.8%, $p < 0.0001$) (Fig. S3). When considering the KASE categories, SV2A levels differed among groups in the hippocampus (e.g. in CA1: $p = 0.0002$) with no significant difference was observed between KASE categories (Fig. 3g). Only a weak association between SV2A levels and TSPO expression was measured (e.g. PIR: $r = -0.420$, $p = 0.032$) (Fig. 3h).

4. Discussion

The present study assessed neuroinflammation in the KASE model of temporal lobe epilepsy by means of TSPO upregulation at disease onset and chronic epilepsy. This study corroborated the extensive neuroinflammation occurring during epileptogenesis as measured non-invasively using TSPO PET imaging, consistent with previous reports by our and other laboratories in different experimental models of TLE (Amhaoul et al., 2015; Bertoglio et al., 2017b; Brackhan et al., 2016, 2018; Dedeurwaerdere et al., 2012; Nguyen et al., 2018; Russmann et al., 2017; Yankam Njiwa et al., 2016).

To our knowledge, this is the first study to classify KASE rats based on their distinctive seizure burden and explore TSPO upregulation at different disease stages. The 3 identified KASE rat categories demonstrated distinct TSPO levels during both early and chronic phases. We have previously shown that TSPO overexpression at 1 to 2 weeks post-*SE* is mainly driven by microglial activation (Amhaoul et al., 2015; Bertoglio et al., 2017a). It is well known that acute neuroinflammation produces a balance of pro- and anti-inflammatory cytokines which can, in turn, polarize microglia to exacerbate or resolve the insult-related damage (Cherry et al., 2014; Therajaran et al., 2020). Thus, the observed higher levels in TSPO in KASE – sporadic SRS rats at disease onset might derive from a higher M2 polarization of microglia in response to the epileptogenic insult, in contrast to chronic neuroinflammation, which is predominantly pro-inflammatory and exacerbates seizure generation (Vezzani et al., 2011). Accordingly, TSPO expression during chronic epilepsy was the highest in the KASE rats with frequent SRS and displayed a positive association between TSPO expression and seizure frequency (e.g. in PIR: $r = 0.826$) consistently with previous observations (Amhaoul et al., 2015; Bogdanovic et al., 2014), suggesting a possible role of TSPO as seizure biomarker during chronic epilepsy (Koepp et al., 2017). However, we did not observe an association between TSPO upregulation during epileptogenesis and chronic disease (e.g. in PIR: $r = -0.05$). The mechanisms underlying the relationship between TSPO upregulation and epileptogenesis are not fully understood yet, nonetheless, based on the current knowledge, it

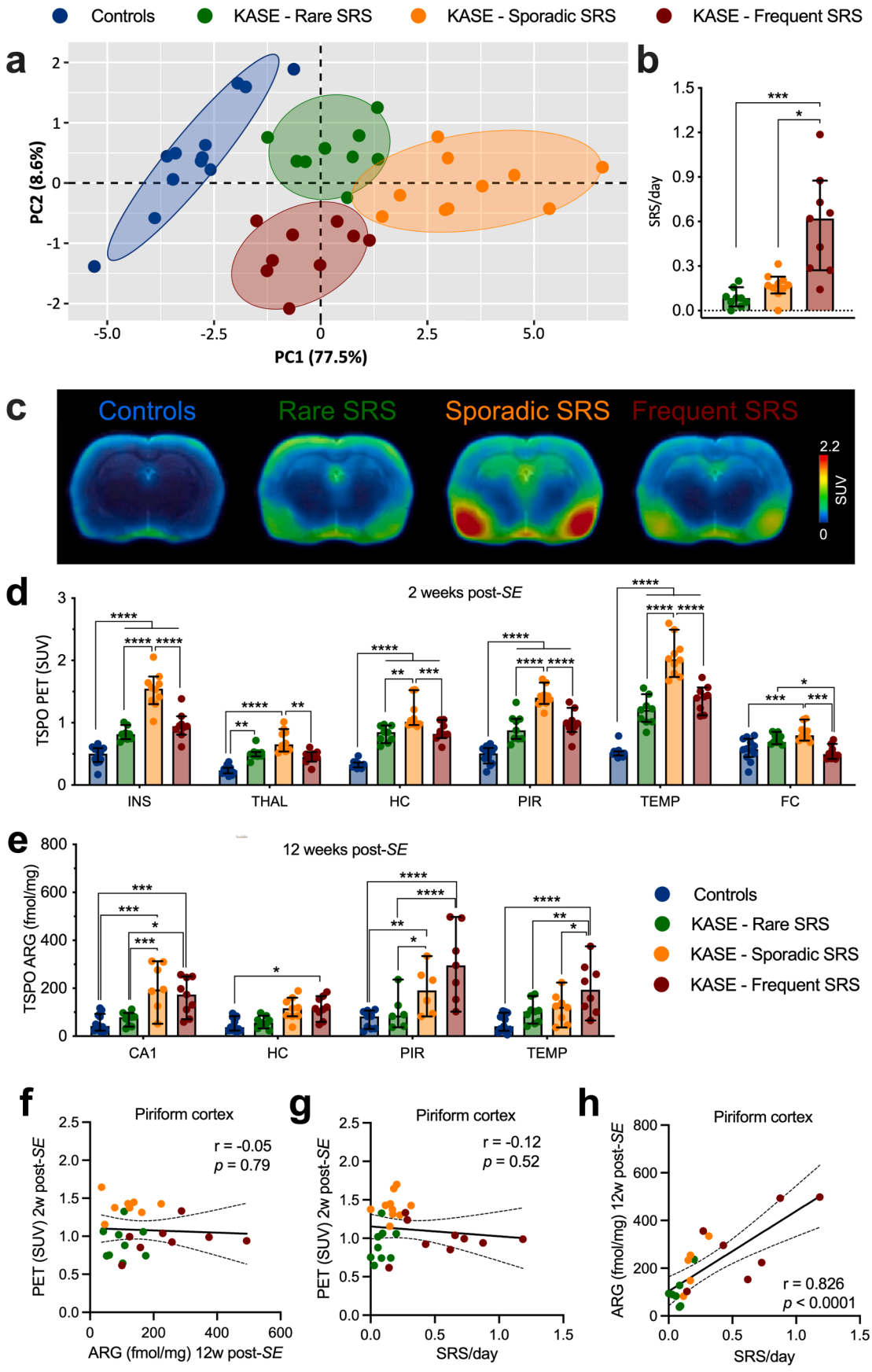

(caption on next page)

Fig. 2. TSPO expression at disease onset identifies KASE categories with distinct seizure burden although independent from chronic TSPO levels. (a) PCA analysis of TSPO PET imaging identified 3 clusters of KASE rats. (b) SRS frequency of the 3 KASE categories estimated using partial least squares applied to the TSPO PET data. (c) Mean [^{18}F]PBR111 SUV PET images for the 4 experimental groups 2 weeks post-*SE*. SUV images are overlaid onto MR images for anatomical localization. (d) TSPO PET quantification 2 weeks post-*SE* showed KASE rats with sporadic SRS displaying the highest uptake. Controls, $n = 12$; KASE – Rare SRS, $n = 9$; KASE – Sporadic SRS, $n = 10$; KASE – Frequent SRS, $n = 9$. (e) TSPO levels 12 weeks post-*SE* increased significantly with the SRS frequency of the KASE rats. Depending on structure: Controls, $n = 10$–12; KASE – Rare SRS, $n = 6$–9; KASE – Sporadic SRS, $n = 6$–10; KASE – Frequent SRS, $n = 7$–9. (f) TSPO levels measured 2 and 12 weeks post-*SE* are not associated. (g) TSPO levels measured at 2 weeks post-*SE* in individual brain structures do not correlate with seizure burden. (h) TSPO levels measured 12 weeks post-*SE* are highly associated with seizure burden. *$p < 0.05$, **$p < 0.01$, ***$p < 0.001$, ****$p < 0.0001$. INS = insular cortex, THAL = thalamus, HC = hippocampus, PIR = piriform cortex, TEMP = temporal lobe, FC = frontal cortex, CA1 = cornu ammonis 1, ARG = autoradiography.

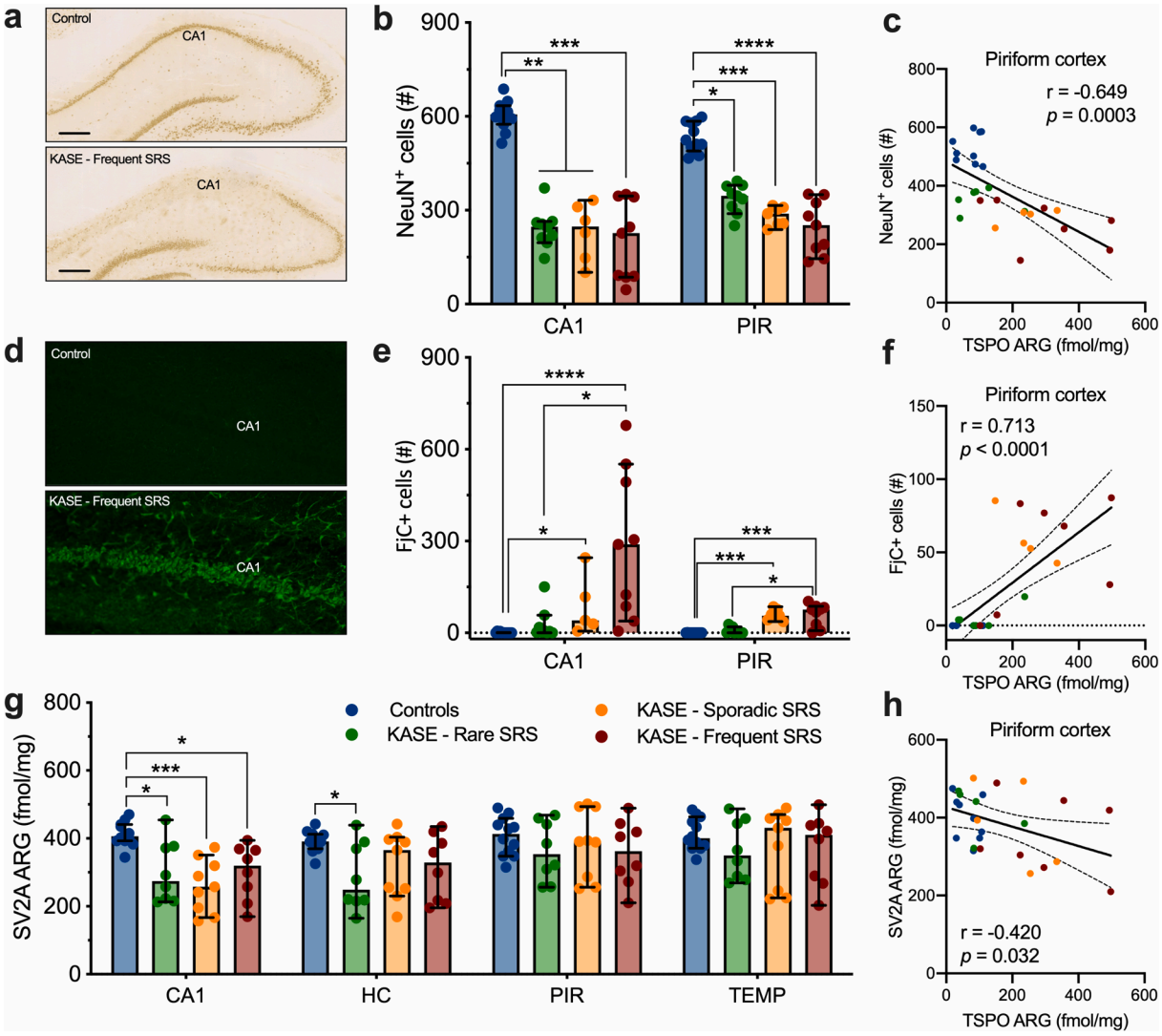

Fig. 3. *Post-mortem* assessment of the different KASE categories during chronic disease. (a) Representative hippocampal NeuN staining of control and KASE – Frequent SRS animal. (b) All 3 KASE categories displayed significant neuronal loss compared to control animals. (c) Correlations between neuronal count and TSPO levels. (d) Representative FjC images in CA1 of control and KASE – Frequent SRS animal. (e) Neurodegeneration increased significantly with the SRS frequency of the KASE rats. (f) Correlations between FjC counts and TSPO levels. (g) SV2A levels 12 weeks post-*SE* were significantly reduced in the CA1 of all KASE categories compared to controls. (h) Correlations between SV2A and TSPO levels. *$p < 0.05$, **$p < 0.01$, ***$p < 0.001$, ****$p < 0.0001$. CA1 = cornu ammonis 1, HC = hippocampus, PIR = piriform cortex, TEMP = temporal lobe, ARG = autoradiography.

appears that TSPO upregulation is driven by different pathophysiological processes superimposed in a two-waves fashion during early and chronic stages of the disease (Fig. 4). On the one hand, the initial wave occurs around 1–2 weeks post-*SE*, depending on the animal model of TLE, and it is characterized by extensive neuroinflammation as a result of epileptogenic changes induced by the initial brain insult (*SE*). On the other hand, the second chronic TSPO wave is associated with the occurrence of seizures in a vicious cycle between neuroinflammation and seizures as previously postulated (Vezzani et al., 2011).

Histological assessment during chronic epilepsy revealed an extensive neuronal loss in all KASE categories. This is not surprising as neuronal loss and seizures are not mutually dependent (Dingledine et al., 2014; Gorter et al., 2003; Pitkanen et al., 2002). Accordingly, we previously demonstrated in this animal model that neuronal loss is extensive already 1-week post-*SE* as a consequence of the initial brain insult (Bertoglio et al., 2017a) and it appears to be continuing into the chronic phase in parallel to higher seizure burden. This could be a direct consequence of the interplay between neuroinflammation and seizure

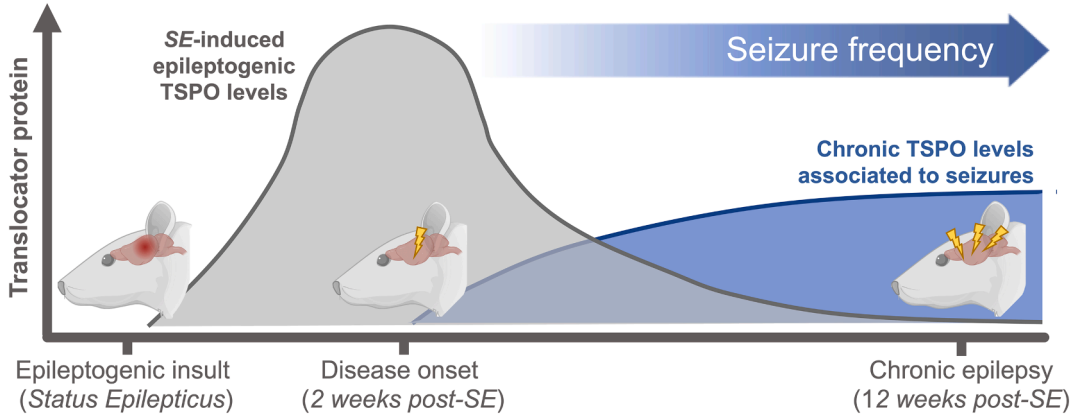

Fig. 4. Hypothesized processes of TSPO upregulation during early and chronic stages of the disease. Following *SE*-induced epileptogenesis, a major TSPO peak occurs around 2 weeks post-*SE*. At this phase, individual brain structures TSPO levels do not reflect the seizure frequency, nonetheless, the multivariate analysis identifies different patterns of TSPO distribution representative of the future seizure burden. During chronic epilepsy, TSPO is upregulated, and its levels in individual brain structures are directly associated with seizure frequency. Figure based on Koepp et al., 2017.

occurrence during chronic epilepsy (Vezzani et al., 2013a, 2011), triggering chronic microglial activation and inducing extensive neurodegeneration (Bertoglio et al., 2017a).

In addition to neuroinflammation, synaptic plasticity and functional remodelling characterize epileptogenesis and chronic epilepsy (Wykes et al., 2019). Accordingly, the hyposynchrony of brain networks during epileptogenesis is associated with the seizure frequency established during chronic epilepsy as recently demonstrated in KASE rats (Bertoglio et al., 2019a; Christiaen et al., 2019). Thus, we utilized [^{3}H]UCB-J autoradiography, a marker of synaptic density, to investigate changes during chronic epilepsy. In the present study, we have demonstrated a declined hippocampal synaptic density during chronic epilepsy, however, it was mainly restricted to the CA1 layer and not associated with seizure frequency. While such focal reduction might be difficult to detect *in vivo* given the spatial resolution of microPET cameras (range of 0.8–1.5 mm), the potential application of SV2A PET imaging as a non-invasive marker for epilepsy is supported by recent work demonstrating its applicability in rodents (Bertoglio et al., 2019b; Thomsen et al., 2020), evidence of reduced synaptic density in KASE rats during the progression of epilepsy (Serrano et al., 2020) and further corroborated by the observation that SV2A PET can detect the epileptogenic focus in patients with refractory TLE (Finnema et al., 2016, 2020).

The development of disease-modifying treatments to alter or even prevent epileptogenesis remains a priority to the field, with identification and validation of non-invasive objective tools to monitor (and predict) disease progression being a key requirement to pursue this goal (Koepp et al., 2017; Pitkanen et al., 2019, 2016). Indeed, the inability to predict disease severity and stratify patients at risk represents is a major shortcoming for the identification of candidate therapeutic targets and selection of subjects to include in anti-epileptogenic therapeutic trials. In this view, the capability of classifying KASE rats on their future distinct seizure frequency based on a single non-invasive TSPO PET scan at disease onset holds great potential. For instance, future studies may focus on investigating distinct expression patterns using RNA sequencing (Hammer et al., 2019) or proteomic profiling (Keck et al., 2017; Walker et al., 2016) between KASE rats with divergent seizure burden (e.g. rare SRS vs frequent SRS) at disease onset to pinpoint novel candidate targets. Additionally, TSPO PET could be implemented as preselection screening of which KASE animals to be included in preclinical anti-epileptogenic trials for the assessment of candidate drugs, significantly reducing the required sample sizes and increasing statistical power, thus increasing their feasibility (Klein and Tyrlikova, 2017; Loscher, 2020).

5. Conclusions

In summary, we found early TSPO upregulation to be associated with epileptogenesis, while chronic TSPO overexpression to be related to seizure frequency. Early and chronic TSPO upregulation following epileptogenic insult appear to be driven by two superimposed dynamic processes, leading to important implications for the assessment of neuroinflammatory therapeutic strategy during disease progression.

CRediT authorship contribution statement

Daniele Bertoglio: Conceptualization, Methodology, Data curation, Investigation, Formal analysis, Funding acquisition, Visualization, Writing - original draft, Writing - review & editing. **Halima Amhaoul:** Conceptualization, Methodology, Data curation, Investigation, Formal analysis, Writing - review & editing. **Joery Goossens:** Data curation, Investigation. **Idrish Ali:** Methodology, Data curation, Investigation, Writing - review & editing. **Elisabeth Jonckers:** Data curation, Investigation. **Tom Bijnens:** Data curation, Investigation. **Matteo Siano:** Data curation, Investigation. **Leonie wyffels:** Investigation, Supervision. **Jeroen Verhaeghe:** Methodology, Software, Supervision, Writing - review & editing. **Annemie Van Linden:** Resources, Supervision, Writing - review & editing. **Steven Staelens:** Resources, Writing - review & editing. **Stefanie Dedeurwaerdere:** Conceptualization, Methodology, Resources, Funding acquisition, Supervision, Writing - review & editing.

Declaration of Competing Interest

The authors declare that they have no known competing financial interests or personal relationships that could have appeared to influence the work reported in this paper.

Acknowledgments

Our gratitude goes to Krystyna Szewczyk, Annemie Van Eetveldt, Philippe Joye, and Caroline Berghmans for the excellent technical assistance. The authors are also thankful to Prof. P. Ponsaerts for providing the fluorescent microscope for FjC analysis. Fig. 4 was created with Biorender.com.

Funding

DB was supported by the Research Foundation Flanders (FWO) (11W2516N/11W2518N as well as 1229721 N). SD was supported by

the FWO funding 1.5.110.14 N, 1.5.144.12 N, ERA-NET NEURON G. A009.13 N, and by the Queen Elisabeth Medical Foundation (Q.E.M.F.) for Neurosciences. MRI equipment was funded by the Flemish Impulse funding for heavy scientific equipment (granted to AVdL; 42/FA010100/1230).

Ethics approval and consent to participate

All procedures were performed according to the European Committee (2010/63/EU) and the Animal Welfare Act (7 USC 2131). All of the animal experiments were approved by the ethical committee for animal testing (ECD 2014-39) at the University of Antwerp (Belgium).

Appendix A. Supplementary data

Supplementary data to this article can be found online at https://doi.org/10.1016/j.nicl.2021.102701.

References

Amhaoul, H., Hamaide, J., Bertoglio, D., Reichel, S.N., Verhaeghe, J., Geerts, E., Van Dam, D., De Deyn, P.P., Kumar-Singh, S., Katsifis, A., Van Der Linden, A., Staelens, S., Dedeurwaerdere, S., 2015. Brain inflammation in a chronic epilepsy model: Evolving pattern of the translocator protein during epileptogenesis. Neurobiol. Dis. 82, 526–539.

Auvin, S., Shin, D., Mazarati, A., Sankar, R., 2010. Inflammation induced by LPS enhances epileptogenesis in immature rat and may be partially reversed by IL1RA. Epilepsia 51 (Suppl 3), 34–38.

Barrett, P.T., Kline, P., 1981. The observation to variable ratio in factor analysis. Personality Study Group Behav. 23–33.

Ben-Ari, Y., 2001. Cell death and synaptic reorganizations produced by seizures. Epilepsia 42 (Suppl 3), 5–7.

Bertoglio, D., Amhaoul, H., Van Eetveldt, A., Houbrechts, R., Van de Vijver, S., Ali, I., Dedeurwaerdere, S., 2017a. Kainic acid-induced post-status epilepticus models of temporal lobe epilepsy with diverging seizure phenotype and neuropathology. Front. Neurol. 8.

Bertoglio, D., Jonckers, E., Ali, I., Verhoye, M., Van der Linden, A., Dedeurwaerdere, S., 2019a. In vivo measurement of brain network connectivity reflects progression and intrinsic disease severity in a model of temporal lobe epilepsy. Neurobiol. Dis. 127, 45–52.

Bertoglio, D., Verhaeghe, J., Miranda, A., Kertesz, I., Cybulska, K., Korat, S., Wyffels, L., Stroobants, S., Mrzljak, L., Dominguez, C., Liu, L., Skinbjerg, M., Munoz-Sanjuan, I., Staelens, S., 2019b. Validation and noninvasive kinetic modeling of [(11)C]UCB-J PET imaging in mice. J. Cereb. Blood Flow Metab. 271678X19864081.

Bertoglio, D., Verhaeghe, J., Santermans, E., Amhaoul, H., Jonckers, E., Wyffels, L., Van Der Linden, A., Hens, N., Staelens, S., Dedeurwaerdere, S., 2017b. Non-invasive PET imaging of brain inflammation at disease onset predicts spontaneous recurrent seizures and reflects comorbidities. Brain Behav. Immun. 61, 69–79.

Bogdanovic, R.M., Syvanen, S., Michler, C., Russmann, V., Eriksson, J., Windhorst, A.D., Lammertsma, A.A., de Lange, E.C., Voskuyl, R.A., Potschka, H., 2014. (R)-[11C]PK11195 brain uptake as a biomarker of inflammation and antiepileptic drug resistance: Evaluation in a rat epilepsy model. Neuropharmacology 85, 104–112.

Bourdier, T., Pham, T.Q., Henderson, D., Jackson, T., Lam, P., Izard, M., Katsifis, A., 2012. Automated radiosynthesis of [18F]PBR111 and [18F]PBR102 using the Tracerlab FXFN and Tracerlab MXFDG module for imaging the peripheral benzodiazepine receptor with PET. Appl. Radiat. Isot. 70, 176–183.

Brackhan, M., Bascunana, P., Postema, J.M., Ross, T.L., Bengel, F.M., Bankstahl, M., Bankstahl, J.P., 2016. Serial quantitative TSPO-targeted PET reveals peak microglial activation up to two weeks after an epileptogenic brain insult. J. Nucl. Med.

Brackhan, M., Bascunana, P., Ross, T.L., Bengel, F.M., Bankstahl, J.P., Bankstahl, M., 2018. [(18) F]GE180 positron emission tomographic imaging indicates a potential double-hit insult in the intrahippocampal kainate mouse model of temporal lobe epilepsy. Epilepsia 59, 617–626.

Cherry, J.D., Olschowka, J.A., O'Banion, M.K., 2014. Neuroinflammation and M2 microglia: the good, the bad, and the inflamed. J. Neuroinflammation 11, 98.

Christiaen, E., Goossens, M.G., Raedt, R., Descamps, B., Larsen, L.E., Craey, E., Carrette, E., Vonck, K., Boon, P., Vanhove, C., 2019. Alterations in the functional brain network in a rat model of epileptogenesis: A longitudinal resting state fMRI study. Neuroimage 202, 116144.

Dedeurwaerdere, S., Callaghan, P.D., Pham, T., Rahardjo, G.L., Amhaoul, H., Berghofer, P., Quinlivan, M., Mattner, F., Loc'h, C., Katsifis, A., Gregoire, M.C., 2012. PET imaging of brain inflammation during early epileptogenesis in a rat model of temporal lobe epilepsy. EJNMMI Res. 2, 60.

Defrise, M., Kinahan, P.E., Townsend, D.W., Michel, C., Sibomana, M., Newport, D.F., 1997. Exact and approximate rebinning algorithms for 3-D PET data. IEEE Trans. Med. Imag. 16, 145–158.

Dingledine, R., Varvel, N.H., Dudek, F.E., 2014. When and how do seizures kill neurons, and is cell death relevant to epileptogenesis? Adv. Exp. Med. Biol. 813, 109–122.

Engel Jr., J., 1996. Introduction to temporal lobe epilepsy. Epilepsy Res. 26, 141–150.

Finnema, S.J., Nabulsi, N.B., Eid, T., Detyniecki, K., Lin, S.F., Chen, M.K., Dhaher, R., Matuskey, D., Baum, E., Holden, D., Spencer, D.D., Mercier, J., Hannestad, J., Huang, Y., Carson, R.E., 2016. Imaging synaptic density in the living human brain. Sci. Transl. Med. 8, 348ra396.

Finnema, S.J., Toyonaga, T., Detyniecki, K., Chen, M.K., Dias, M., Wang, Q., Lin, S.F., Naganawa, M., Gallezot, J.D., Lu, Y., Nabulsi, N.B., Huang, Y., Spencer, D.D., Carson, R.E., 2020. Reduced synaptic vesicle protein 2A binding in temporal lobe epilepsy: A [(11) C]UCB-J positron emission tomography study. Epilepsia.

Goffin, K., Dedeurwaerdere, S., Van Laere, K., Van Paesschen, W., 2008. Neuronuclear assessment of patients with epilepsy. Semin. Nucl. Me.d 38, 227–239.

Gomez-Carracedo, M.P., Andrade, J.M., Rutledge, D.N., Faber, N.M., 2007. Selecting the optimum number of partial least squares components for the calibration of attenuated total reflectance-mid-infrared spectra of undesigned kerosene samples. Anal. Chim. Acta 585, 253–265.

Gorter, J.A., Goncalves Pereira, P.M., van Vliet, E.A., Aronica, E., Lopes da Silva, F.H., Lucassen, P.J., 2003. Neuronal cell death in a rat model for mesial temporal lobe epilepsy is induced by the initial status epilepticus and not by later repeated spontaneous seizures. Epilepsia 44, 647–658.

Hammer, M.F., Sprissler, R., Bina, R.W., Lau, B., Johnstone, L., Walter, C.M., Labiner, D. M., Weinand, M.E., 2019. Altered expression of signaling pathways regulating neuronal excitability in hippocampal tissue of temporal lobe epilepsy patients with low and high seizure frequency. Epilepsy Res. 155, 106145.

Hudson, H.M., Larkin, R.S., 1994. Accelerated image reconstruction using ordered subsets of projection data. IEEE Trans. Med. Imag. 13, 601–609.

Keck, M., Androsova, G., Gualtieri, F., Walker, A., von Ruden, E.L., Russmann, V., Deeg, C.A., Hauck, S.M., Krause, R., Potschka, H., 2017. A systems level analysis of epileptogenesis-associated proteome alterations. Neurobiol. Dis. 105, 164–178.

Keezer, M.R., Sisodiya, S.M., Sander, J.W., 2016. Comorbidities of epilepsy: current concepts and future perspectives. Lancet Neurol. 15, 106–115.

Klein, P., Tyrlikova, I., 2017. Prevention of epilepsy: Should we be avoiding clinical trials? Epilepsy Behav. 72, 188–194.

Koepp, M.J., Arstad, E., Bankstahl, J.P., Dedeurwaerdere, S., Friedman, A., Potschka, H., Ravizza, T., Theodore, W.H., Baram, T.Z., 2017. Neuroinflammation imaging markers for epileptogenesis. Epilepsia 58 (Suppl 3), 11–19.

Levesque, M., Avoli, M., 2013. The kainic acid model of temporal lobe epilepsy. Neurosci. Biobehav. Rev. 37, 2887–2899.

Lillis, K.P., Wang, Z., Mail, M., Zhao, G.Q., Berdichevsky, Y., Bacskai, B., Staley, K.J., 2015. Evolution of network synchronization during early epileptogenesis parallels synaptic circuit alterations. J. Neurosci. 35, 9920–9934.

Loscher, W., 2020. The holy grail of epilepsy prevention: Preclinical approaches to antiepileptogenic treatments. Neuropharmacology 167, 107605.

Naes, T., Martens, H., 1985. Comparison of prediction methods for multicollinear data. Commun. Stat. – Simul. Comput. 14, 545–576.

Nguyen, D.L., Wimberley, C., Truillet, C., Jego, B., Caille, F., Pottier, G., Boisgard, R., Buvat, I., Bouilleret, V., 2018. Longitudinal positron emission tomography imaging of glial cell activation in a mouse model of mesial temporal lobe epilepsy: Toward identification of optimal treatment windows. Epilepsia 59, 1234–1244.

Paxinos, G., Watson, C., 2007. The rat brain in stereotaxic coordinates, Sixth edition ed. Elsevier Inc.

Pernot, F., Heinrich, C., Barbier, L., Peinnequin, A., Carpentier, P., Dhote, F., Baille, V., Beaup, C., Depaulis, A., Dorandeu, F., 2011. Inflammatory changes during epileptogenesis and spontaneous seizures in a mouse model of mesiotemporal lobe epilepsy. Epilepsia 52, 2315–2325.

Pitkanen, A., Ekolle Ndode-Ekane, X., Lapinlampi, N., Puhakka, N., 2019. Epilepsy biomarkers - Toward etiology and pathology specificity. Neurobiol Dis 123, 42–58.

Pitkanen, A., Engel Jr., J., 2014. Past and present definitions of epileptogenesis and its biomarkers. Neurotherapeutics 11, 231–241.

Pitkanen, A., Loscher, W., Vezzani, A., Becker, A.J., Simonato, M., Lukasiuk, K., Grohn, O., Bankstahl, J.P., Friedman, A., Aronica, E., Gorter, J.A., Ravizza, T., Sisodiya, S.M., Kokaia, M., Beck, H., 2016. Advances in the development of biomarkers for epilepsy. Lancet Neurol. 15, 843–856.

Pitkanen, A., Lukasiuk, K., Dudek, F.E., Staley, K.J., 2015. Epileptogenesis. Cold Spring Harb Perspect Med 5.

Pitkanen, A., Nissinen, J., Nairismagi, J., Lukasiuk, K., Grohn, O.H., Miettinen, R., Kauppinen, R., 2002. Progression of neuronal damage after status epilepticus and during spontaneous seizures in a rat model of temporal lobe epilepsy. Prog. Brain Res. 135, 67–83.

Racine, R.J., 1972. Modification of seizure activity by electrical stimulation II. Motor seizure. Electroencephalogr Clin. Neurophysiol. 32, 281–294.

Ravizza, T., Balosso, S., Vezzani, A., 2011. Inflammation and prevention of epileptogenesis. Neurosci. Lett. 497, 223–230.

Rupprecht, R., Papadopoulos, V., Rammes, G., Baghai, T.C., Fan, J., Akula, N., Groyer, G., Adams, D., Schumacher, M., 2010. Translocator protein (18 kDa) (TSPO) as a therapeutic target for neurological and psychiatric disorders. Nat. Rev. Drug Discov. 9, 971–988.

Russmann, V., Brendel, M., Mille, E., Helm-Vicidomini, A., Beck, R., Gunther, L., Lindner, S., Rominger, A., Keck, M., Salvamoser, J.D., Albert, N.L., Bartenstein, P., Potschka, H., 2017. Identification of brain regions predicting epileptogenesis by serial [18F]GE-180 positron emission tomography imaging of neuroinflammation in a rat model of temporal lobe epilepsy. Neuroimage Clin. 15, 35–44.

Schmued, L.C., Stowers, C.C., Scallet, A.C., Xu, L., 2005. Fluoro-Jade C results in ultra high resolution and contrast labeling of degenerating neurons. Brain Res. 1035, 24–31.

Serrano, M.E., Bahri, M.A., Becker, G., Seret, A., Germonpre, C., Lemaire, C., Giacomelli, F., Mievis, F., Luxen, A., Salmon, E., Rogister, B., Raedt, R., Plenevaux, A., 2020. Exploring with [(18)F]UCB-H the in vivo Variations in SV2A

Expression through the Kainic Acid Rat Model of Temporal Lobe Epilepsy. Mol. Imag. Biol.
Tellez-Zenteno, J.F., Hernandez-Ronquillo, L., 2012. A review of the epidemiology of temporal lobe epilepsy. Epilepsy Res. Treat. 2012, 630853.
Therajaran, P., Hamilton, J.A., O'Brien, T.J., Jones, N.C., Ali, I., 2020. Microglial polarization in posttraumatic epilepsy: Potential mechanism and treatment opportunity. Epilepsia 61, 203–215.
Thomsen, M.B., Jacobsen, J., Lillethorup, T.P., Schacht, A.C., Simonsen, M., Romero-Ramos, M., Brooks, D.J., Landau, A.M., 2020. In vivo imaging of synaptic SV2A protein density in healthy and striatal-lesioned rats with [11C]UCB-J PET. J. Cereb. Blood Flow Metab. 271678X20931140.
Vezzani, A., Aronica, E., Mazarati, A., Pittman, Q.J., 2013a. Epilepsy and brain inflammation. Exp. Neurol. 244, 11–21.
Vezzani, A., French, J., Bartfai, T., Baram, T.Z., 2011. The role of inflammation in epilepsy. Nat. Rev. Neurol. 7, 31–40.
Vezzani, A., Friedman, A., 2011. Brain inflammation as a biomarker in epilepsy. Biomark Med. 5, 607–614.
Vezzani, A., Friedman, A., Dingledine, R.J., 2013b. The role of inflammation in epileptogenesis. Neuropharmacology 69, 16–24.
Walker, A., Russmann, V., Deeg, C.A., von Toerne, C., Kleinwort, K.J., Szober, C., Rettenbeck, M.L., von Ruden, E.L., Goc, J., Ongerth, T., Boes, K., Salvamoser, J.D., Vezzani, A., Hauck, S.M., Potschka, H., 2016. Proteomic profiling of epileptogenesis in a rat model: Focus on inflammation. Brain Behav. Immun. 53, 138–158.
Williams, P.A., White, A.M., Clark, S., Ferraro, D.J., Swiercz, W., Staley, K.J., Dudek, F. E., 2009. Development of spontaneous recurrent seizures after kainate-induced status epilepticus. J. Neurosci. 29, 2103–2112.
Wykes, R.C., Khoo, H.M., Caciagli, L., Blumenfeld, H., Golshani, P., Kapur, J., Stern, J.M., Bernasconi, A., Dedeurwaerdere, S., Bernasconi, N., 2019. WONOEP appraisal: Network concept from an imaging perspective. Epilepsia 60, 1293–1305.
Yankam Njiwa, J., Costes, N., Bouillot, C., Bouvard, S., Fieux, S., Becker, G., Levigoureux, E., Kocevar, G., Stamile, C., Langlois, J.B., Bolbos, R., Bonnet, C., Bezin, L., Zimmer, L., Hammers, A., 2016. Quantitative longitudinal imaging of activated microglia as a marker of inflammation in the pilocarpine rat model of epilepsy using [11C]-(R)-PK11195 PET and MRI. J. Cereb. Blood Flow Metab.

Author/s:
Bertoglio, D; Amhaoul, H; Goossens, J; Ali, I; Jonckers, E; Bijnens, T; Siano, M; Wyffels, L; Verhaeghe, J; Van Der Linden, A; Staelens, S; Dedeurwaerdere, S

Title:
TSPO PET upregulation predicts epileptic phenotype at disease onset independently from chronic TSPO expression in a rat model of temporal lobe epilepsy

Date:
2021-01-01

Citation:
Bertoglio, D., Amhaoul, H., Goossens, J., Ali, I., Jonckers, E., Bijnens, T., Siano, M., Wyffels, L., Verhaeghe, J., Van Der Linden, A., Staelens, S. & Dedeurwaerdere, S. (2021). TSPO PET upregulation predicts epileptic phenotype at disease onset independently from chronic TSPO expression in a rat model of temporal lobe epilepsy. NEUROIMAGE-CLINICAL, 31, https://doi.org/10.1016/j.nicl.2021.102701.